HOKKAIDO UNIVERSITY

Title	Thermal aging of acrylic-urethane network: Kinetic modeling and end-of-life criteria combined with mechanical properties
Author(s)	Ishida, Takato; Richaud, Emmanuel; Gervais, Matthieu et al.
Citation	Progress in Organic Coatings, 163, 106654 https://doi.org/10.1016/j.porgcoat.2021.106654
Issue Date	2022-02
Doc URL	https://hdl.handle.net/2115/90927
Rights	© <2022>. This manuscript version is made available under the CC-BY-NC-ND 4.0 license https://creativecommons.org/licenses/by-nc-nd/4.0/
Rights(URL)	https://creativecommons.org/licenses/by-nc-nd/4.0/
Type	journal article
File Information	Press_version_manuscript20211204.pdf

Hokkaido University Collection of Scholarly and Academic Papers : HUSCAP

Thermal aging of acrylic-urethane network: kinetic modeling and end-of-life criteria combined with mechanical properties

Takato ISHIDA[a*, c], Emmanuel RICHAUD[b], Matthieu GERVAIS[b], Alain GAUDY[b], Ryoma KITAGAKI[a], Hideaki HAGIHARA[c], Yogarajah ELAKNESWARAN[a]

a Graduate School of Engineering, Hokkaido University, Nishi-8-chome, Kita-13-jyo, Kita-ku, Sapporo-shi, Hokkaido 060-8628, Japan

b Laboratoire PIMM, Arts et Metiers Institute of Technology, CNRS, Cnam, HESAM Universite, 151 bd de Hôpital, 75013 Paris, France

c Research Institute for Sustainable Chemistry, National Institute of Advanced Industrial Science and Technology (AIST), Tsukuba, Ibaraki 305-8565, Japan

a* E-mail: takato.matphysichem@gmail.com (T. Ishida)

Abstract

This study addresses the multiscale analysis of acrylic urethane networks (AUN). To establish the

kinetic model for predicting AUN oxidation, this study considered the pure thermal oxidation of AUN at 160, 180, and 200 °C. Chemical changes were monitored using infrared spectroscopy. These indicated the presence of an imide, presumably generated from the oxidation of CH_2 at the α-position of nitrogen. On the macromolecular and macroscopic scales, oxidation was shown to induce predominant crosslinking, leading to a drop in toughness (i.e., embrittlement). The novel kinetic model of AUN thermal aging was developed from a mechanistic scheme previously established for polyamide 11, by adding some extra paths of thermolytic alkyl radical formation, oxidative N-H bonds decomposition and coupling of aminyl radicals.

Keywords: Kinetics, oxidation, macromolecular architecture, acrylic-urethane network

1. Introduction

Acrylic-urethane network (AUN) is a well-known thermoset material used in a wide variety of commercial and technical applications; it is particularly prevalent as a coating for buildings and infrastructure, owing to its excellent flexibility, film-forming properties, and resistance to weathering [1]. The coatings applied to structure surfaces are exposed to several environmental stress factors, such as temperature [2], light [3], water [4], and oxygen [5,6]. They perform a significant role as a barrier material inhibiting the penetration of CO_2, moisture and chloride ions to protect concrete and steel from corrosion and increase the durability of buildings and infrastructure [1,7,8]. Hence, good barrier properties are required for the coatings.

Cracking is a major problem for coatings, and it can ultimately determine the lifespan of structures. Cracking phenomena have been widely studied and have attracted attention from coating users in the building and construction communities, because cracking failure can induce a dramatic deterioration of crucial building properties [9,10].

For evaluating the resistance to crack propagation, the Essential Work of Fracture (EWF) method [11,12] should be the first choice, which analyzes the fracture properties of notched specimens. As one of the alternative options, it is sometimes evaluated from the area under the stress–strain curve [13] of the classical tensile test, a routine procedure for characterizing mechanical properties in the polymer degradation field [4,14,15]. This loss of ductility is related to various macromolecular characteristics such as internal stress [11], changes in crosslink density [16], fracture energy [17], and changes in sample weight due to the release of small volatile products [18].

In real applications of polymer-based materials, oxidation strongly limits the service lifetime, because oxidized materials suffer deteriorations (e.g., embrittlement and yellowing) in their structural properties. In general, oxidation modifies not only the chemical structure but also the macromolecular architecture [19] through chain scission and/or crosslinking [20,21]. Hence, a multi-scale perspective is needed to understand aging behaviors and service lifetimes.

AUN oxidation has been studied in earlier papers on photo-aging [22–25]. Oxidation of urethane group was highlighted together with a predominant crosslinking (which increases the glass transition temperature

(T_g) and micro-hardness [22]) and a decrease in the free volume and its radius [23]. An elaborated kinetic model for lifetime prediction would represent a valuable tool for AUN users and manufacturers. However, it is difficult to construct a kinetic model for photothermal oxidation from scratch, because photo-oxidation involves complex radical initiation processes determined by the wavelength dependence of the UV-light's effects and the presence of additional physical phenomena such as light attenuation across the material's thickness. In the case of the polypropylene, a kinetic model for photooxidation was developed by completing the model for thermal oxidation [26]. The first aim of this work is an experimental multiscale study of AUN thermal aging since those latter are uncommon in the literature. This study also aims to establish a novel kinetic model for thermal aging (in accordance with Refs. [18] [19][27]) and to investigate the end-of-life criteria related to mechanical resistance.

2. Experimental

2.1 Materials

The target material was a two-part acrylic-urethane paint (acrylic-polyol and crosslinker) designed for commercial use; it consists of a tri-functional network structure cross-linked by hexamethylene diisocyanate trimer (HDI). No additives or stabilizers were added to the samples. The chemical structure of the acrylic-polyol (M_n = 7000 [g/mol]) was obtained by pyrolysis gas chromatography–mass spectrometry, and nuclear magnetic resonance (NMR) analysis, as described in our previous work [28]. As

shown in Fig. 1(a), acrylic-polyol is composed of methyl methacrylate (MMA), styrene (St), butyl acrylate (BuA), and 2-hydroxyethyl methacrylate (HMA). The approximate composition stoichiometry of acrylic-polyol can be inferred from the NMR results, as follows: [MMA]:[St]:[BuA]:[HMA] ~ 0.32:0.36:0.16:0.16.

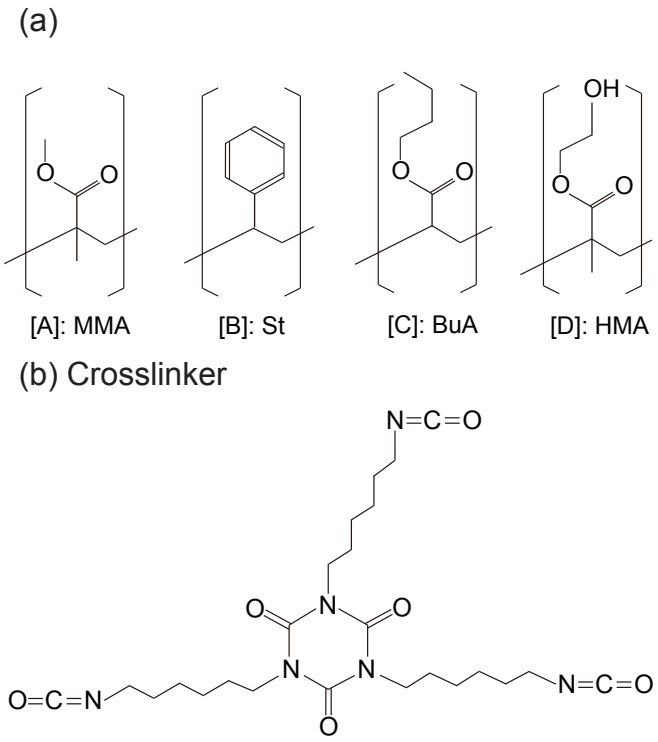


Fig. 1. (a) Structural units of acrylic polyol and (b) chemical structure of crosslinker (HDI trimer).

[(1-column fitting image)].

Solutions of polyol and crosslinker were mixed in a given polyol/hardener weight ratio of 17/5. The concentrations of OH and NCO in the mixed solution were approximately $[OH]_{mix} \sim 1.30$ [mol/kg] and

$[NCO]_{mix} \sim 1.35$ [mol/kg], respectively.

2.1.1 Preparation of film samples

Two-component mixed solutions were cast on a Naflon® sheet (Nichias, Japan) to allow the film sample to be easily peeled off. The samples were hardened under dry conditions (i.e., a desiccator containing silica gel) at 20 °C for a week, after which they were placed in an oven at 105 °C for 2 h. The thicknesses of the film samples were approximately 50–100 μm (measured by ultrasonic thickness gauge, SDM-3100, SANKO Electronic Laboratory Co. Ltd., Japan). The samples were fully cured, as verified by the total disappearance of the peak at 2275 cm^{-1} (attributed to the isocyanate group) in the Fourier transform infrared (FTIR) spectra, as described in our previous work [28]. Concerning the so-called "diffusion limited oxidation (DLO)" effect [29,30], Larché, Bussière, and Gardette [22] studied the photo-oxidation of approximately 40–60 μm acrylic-urethane thin films to investigate the material's photo-oxidation behavior. Accordingly, we assumed that the oxidation behavior of our thin films (50–100 μm thickness) was not DLO-controlled in this work.

2.2 Thermal-aging tests

Sample films were placed in air-ventilated AP60 ovens (supplied by Systèmes Climatique Service, France) at temperatures of 160–200 °C.

2.3 Characterization

2.3.1 Fourier-transform infrared spectroscopy (FTIR)

Infrared (IR) spectra were collected in transmission mode using a Frontier spectrophotometer (supplied by Perkin Elmer). The spectra were averaged over 64 scans at a resolution of 4 cm^{-1} in the range 400–4000 cm^{-1}. The concentrations of the oxidation products were calculated using the Lambert–Beer law, expressed as

$$A = \varepsilon_\lambda \times l \times C_\lambda, \quad (1)$$

where A is the absorbance, ε_λ [$L \cdot mol^{-1} \cdot cm^{-1}$] is the molar extinction coefficient, l is the sample thickness [cm], and C_λ is the concentration of the target chemical species [$mol \cdot L^{-1}$]. Here, we took the value reported in the literature: $\varepsilon(Imide) = 285$ $L \cdot mol^{-1} \cdot cm^{-1}$. [19]

2.3.2 Classical tensile experiment

The mechanical changes induced by the oxidation of the AUN were captured by tensile testing on an Instron® 4301 machine. Dumbell samples were obtained by punching the AUN films. The effective zone had dimensions of 10 mm (length) and 2 mm (width). The crosshead speed was held constant at 1 mm/min

during the test, and a 100 N cell was used.

2.3.3 Dynamic Mechanical Analysis (DMA)

The dynamic mechanical analysis (DMA) measurements were performed on a Q800 apparatus (TA instruments) driven by a Qseries Explorer in the tensile mode, within a temperature range of 40–140 °C using virgin or aged AUN films. The measurement frequency was 1 Hz, and the heating rate was 3 °C/min under a strain of 0.2% with a 0.004 N preload force.

2.3.4 Sol-gel analysis

Swelling experiments were performed using the classical gravimetric method; for this, virgin and aged samples were immersed (initial mass m_0) in toluene at room temperature. After reaching the equilibrium swelling states, the samples were removed and lightly wiped with tissue to remove excess solvent from their surfaces. Then, the samples were dried under vacuum conditions until an equilibrium was reached (mass: m_{dry}). The data were used to estimate the soluble fraction (SF), as follows:

$$SF = \frac{m_0 - m_{dry}}{m_0}. \quad (2)$$

The swelling degree (Q) was formulated as described in [23]:

$$Q = \frac{m_s - m_{dry}}{m_{dry}}. \quad (3)$$

Here, Q is the swelling degree in the equilibrium state, and m_s is the weight of the sample after swelling.

2.3.5 Pyrolysis gas chromatography–mass spectrometry (GC/MS) analysis

A sample of approximately 1 mg was used for the pyrolysis gas chromatography–mass spectrometry (GC/MS) measurements. The sample was placed in a deactivated stainless-steel sample cup and heated in a pyrolyzer at 200 ° C for 6 h under a helium atmosphere with a flow rate of 50 mL/min. The resultant volatiles were redirected to a GC/MS system (GCMS-QP2010 SE, Shimadzu, Kyoto, Japan). A proportion of the flow (1 mL/min), reduced by the GC splitter (50:1), was continuously introduced into the MS via a transfer capillary. This capillary was maintained at 280 ° C in a GC oven to prevent condensation of less volatile products in the capillary (Ultra ALLOY, 0.25 mm i.d. × 30 m long, Frontier Lab). For the MS measurements, electro-ionization was performed at 70 eV with an operating mass range of 20–500 *m/z* and a scan rate of 0.3 s/scan. Observed products were identified using the corresponding mass spectra and the F-search software (Frontier Laboratories Ltd).

2.3.6 Differential Scanning Calorimetry (DSC)

Differential scanning calorimetry (DSC) was conducted using a Q10 apparatus (TA Instruments). Approximately 5 mg of each sample was placed in a standard sealed aluminum pan and heated from 0 to 200 °C at a heating rate of 10 °C/min. The DSC cell was continuously purged with nitrogen (50 ml/min). The results were analyzed using TA Analysis software.

2.3.7 Nuclear Magnetic Resonance (NMR)

^{1}H-NMR spectra for virgin/aged polyol (linear) components at 200 °C under air and vacuum conditions were collected. The samples dissolved in $CDCl_3$ solution measured at room temperature on a Bruker Avance III HD400 spectrometer (400 MHz) using standard pulse sequences available in the Bruker software. Chemical shifts are expressed relative to $SiMe_4$, which is used as an internal reference.

3. Results

3.1 Chemical changes

Chemical change monitoring should constitute the first step in a mechanistic discussion of thermal aging behavior. In general, the thermal oxidation loop is initiated by thermolysis of the peroxide groups [19,22,27,31]. In addition, homolysis of urethane groups were previously reported under both conditions in heating and UV irradiation [32,33]. We expect the thermal aging at high temperatures (in the range of

160–200 °C) can provide insight into both oxidative and non-oxidative degradation chemistry of AUN. Although alkyl radicals ($P°$) can be formed during thermal oxidation via the hydrogen abstraction of peroxy radicals ($POO°$), the non-oxidative route of $P°$ formation from thermolytic events of the main functional groups must be investigated in thermal aging cases. Here, we study preliminary thermal aging under vacuum conditions at 200 °C, followed by FTIR (Fig. S1 in the Supplementary Materials). Even in the case of inert thermal aging, thermolytic scission of the N–H bonds was not observed.

Next, the time-dependent IR spectra for thermal aging under air are shown in Fig. 2 (a)–(f). The peak absorption correspondences in Fig. 2 were determined from the literature [3,23,34,35] and by comparisons of the FTIR spectra of casted polyol and AUN films (see Fig. S2 in the Supplementary Materials). The bands at 3385 cm^{-1} and the shoulder of the C–H region at 2859 cm^{-1} are attributed to the N–H stretching vibration in urethane-linkage and C–H bonds at the α-position of an N atom. Absorption in the region 1850–1650 cm^{-1} region corresponds to C=O vibrations. The vibrational band at 1539 cm^{-1} represents the amide II band, which indicates a combination of C–N stretching and N–H in-plane-bending vibrations. First of all, the formation of a left-wing of the C=O band (1800–1750 cm^{-1}) clearly indicates the progress of oxidation [2,3,19,22,23,36]. This wide band at 1800–1750 cm^{-1} is quite complex because of overlapping peaks of oxidized products; however, it may contain a possible indicator of AUN oxidation. In general, it is commonly concluded that the features of urethane oxidation include an N–H group (urethane) loss, consumption of C–H bonds at the α-position of an N atom, development of the band at 1770 cm^{-1}

1 (attributable for the oxidized product, imide structure), and loss of the amide II band [2,22,23,37]. In
2 addition, a very small peak at 3240 cm^{-1} appeared in Fig. 2(a) also corresponds to an N-H bond in the
3 generated imide structure [38]. On the other hand, a formation of the shoulder at 1800–1780 cm^{-1} in the
4 severely aged cases possibly implies the oxidation of the acrylic-polyol part (attributed to anhydride and/or
5 lactone) [39,40]. These mechanisms are discussed in detail in the Discussion section (with reference to
6 previous investigations). Furthermore, the decrease of absorbance at 3385 cm^{-1} suggests that N-H groups
7 in urethane are destroyed and aminyl radicals are formed [41]. It is well known that the bond dissociation
8 energy (BDE) values for the N-H bond and the C–H bond at the α-position of the heteroatoms were
9 significantly lower than those for the C–H bond in olefinic materials [31,42]. From observed spectral
10 features in thermal aging, possible structures of alkyl radicals and aminyl radicals can be considered around
11 heteroatoms in this system (i.e., urethane-linkage and isocyanurate ring), as shown in Scheme. 1.
12

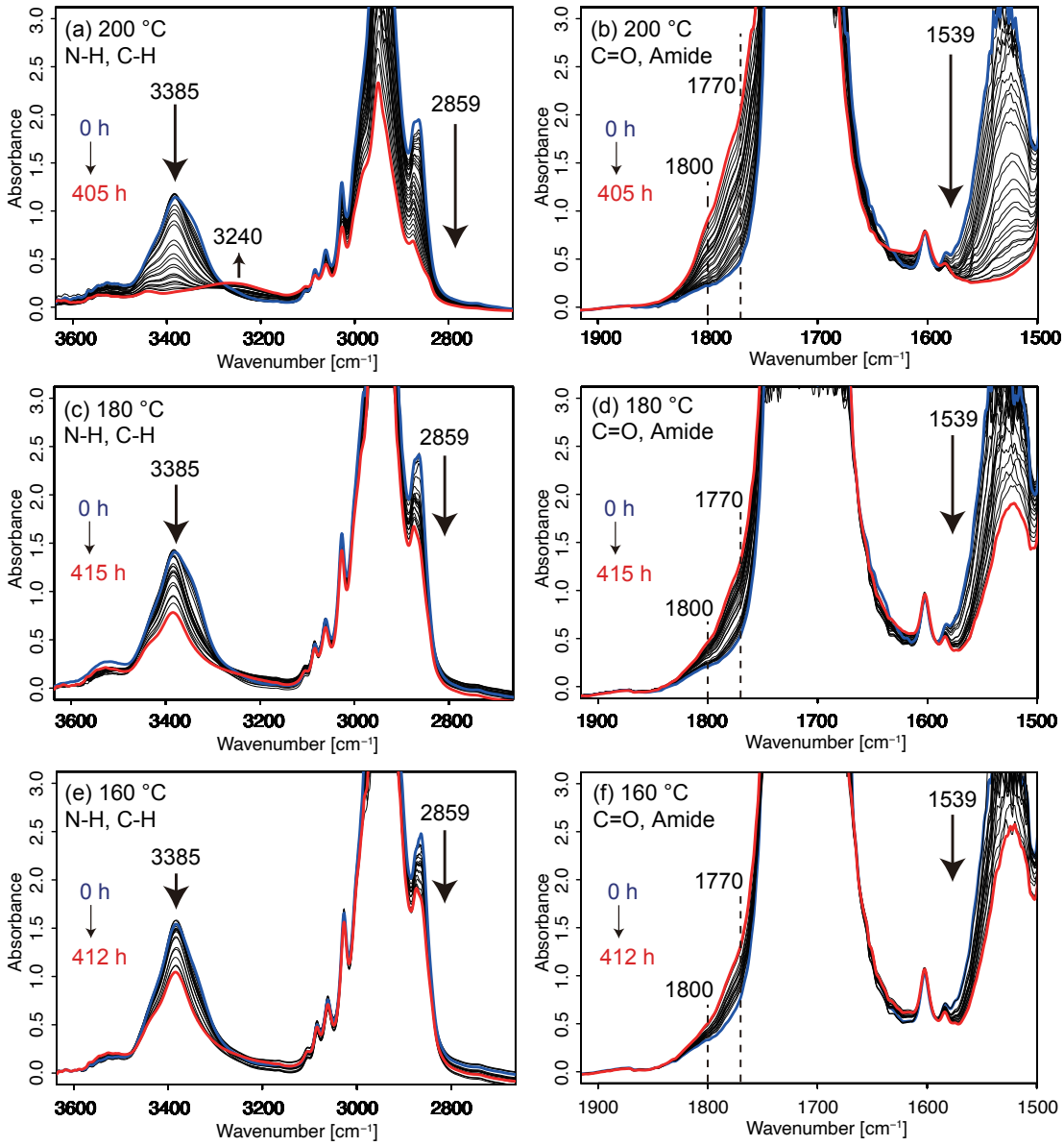
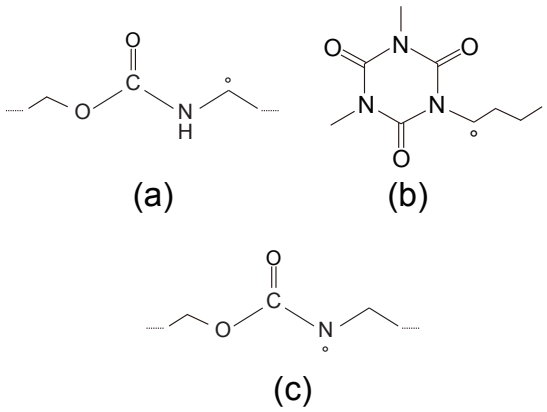


Fig. 2. Time-dependent IR spectra for thermally aging AUN at (a), (b) 200 °C;

(c), (d) 180 °C; and (e), (f) 160 °C under air.

[(Color), (2-column fitting image)].



Scheme 1. Possible structures of radicals around heteroatoms.

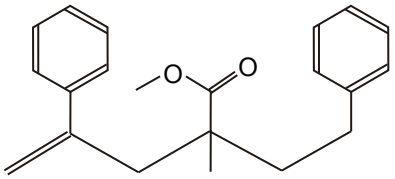
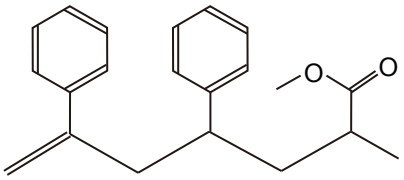
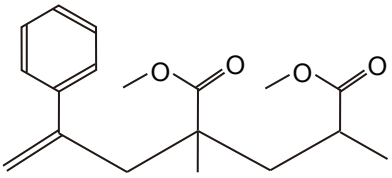
(a), (b): alkyl radicals, (c): aminyl radical

[(1-column fitting image)].

To identify volatile compounds, GC/MS measurements were performed. Volatiles were collected from samples heated in the pyrolyzer at 200° C for 6 h under a helium atmosphere. The pyrogram observed for this measurement in the total ion current (TIC) mode is shown in Fig. S3 in the Supplementary Materials. The assigned products listed in Table. 1 indicate the volatilization of the styrenic and MMA units from the acrylic linear component. Note that these fragments were not observed in case of flash pyrolysis at 200° C, adsorbed water and monomer-dissolving solvents could be only detected. In other word, these fragments were not ascribed for unreacted monomers but cleaved product from AUN system. In addition, the BuA unit was not detected in this GC/MS measurement. This may be because the amount of unstable BuA unit was small, or the unit is thermally more stable than the detected the trimer fragments (e.g., St-St-MMA unit, St-MMA-St unit, St-MMA-MMA). Note that no units were detected in the

monomeric or dimeric state in the short retention time region on the pyrogram (Fig. S3 in the Supplementary Materials.). It may be that the part of the trimer consisting of MMA and St is thermally unstable and easily ejected, and BuA is possibly not included in the unstable part. Hence, these trimer fragments consisting of MMA and St are potentially responsible for mass loss in the AUN system. This is discussed in the Discussion section (along with the mass-loss behavior).

Table. 1. Main volatiles identified from GC/MS analysis.

Retention time [min]	Origin	Formula
14.9, 15.1, 16.3	St dimer and MMA	
15.0, 15.2, 15.7	St dimer and MMA	
16.1, 16.2	St and MMA dimer	

3.2. Macromolecular changes

The mass losses obtained for aging under air at several temperatures (160, 180, and 200 °C) are shown in Fig. 3 for the crosslinked AUN and (un-crosslinked) polyol film. Furthermore, we compared AUN

thermally aged at 200 °C under air and under vacuum.

The results suggest the following comments:

- Mass-loss curves systematically display a very rapid mass-loss stage, which is typically ascribed to absorbed water, and monomer-dissolving solvents [43,44].

- The entire curve exhibits the auto-decelerated shape typical of oxidation processes involving reactive sites in the α-position of heteroatoms [2,27].

- For all aging conditions under air (200 °C, 180 °C, and 160 °C), the mass-loss curves are relatively similar for linear polyol and AUN. More precisely, the mass loss was slightly higher for the polyol component. Expressed otherwise, the reactions responsible for the release of volatiles primarily occur in the acrylic-polyol component, which coincides with the detected volatile compounds in the GC/MS measurement.

- The comparison of aging under air and vacuum conditions at 200 °C suggests that thermal degradation under vacuum generates only a small number of chain scissions and (later) volatile compounds, as discussed below.

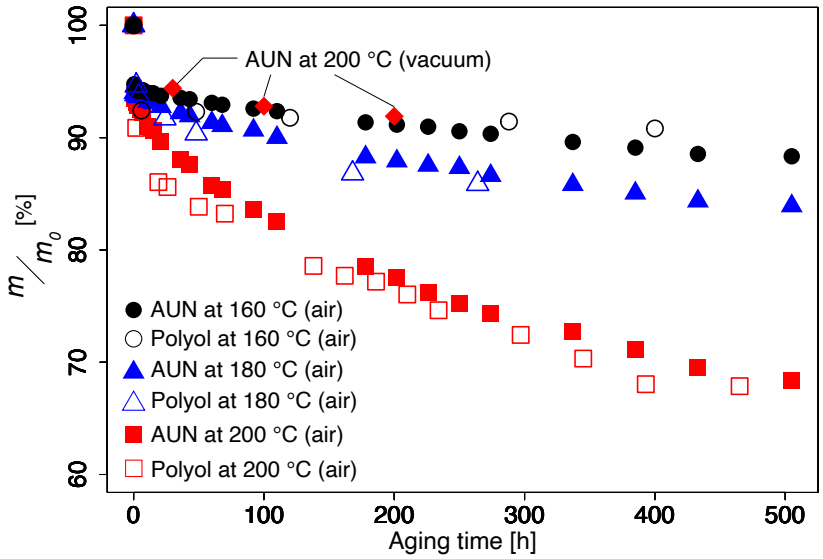


Fig. 3. Mass-loss behaviors under thermal aging at 160°C, 180°C, and 200°C for AUN and polyol under air and vacuum (closed symbols correspond to AUN, open symbols to polyol).

[(Color), (1-column fitting image)].

These investigations were completed by measuring the glass transition from the temperature (T_g) of AUN for aging under air (at 160, 180, and 200°C) and vacuum (at 200°C) conditions. To begin with, a comparison of T_g changes at 200°C under air and vacuum conditions was performed via DSC measurements, as shown in Fig. 4(a). Accordingly, the T_g values increased under both aging conditions (i.e., both air and vacuum conditions). Figure 4(b) illustrates the aging-temperature dependence of the change in T_g, which was assessed by DMA measurements. In addition to the results shown in Fig. 4(a), T_g actually increased for all studied aging conditions. Firstly, rapid T_g increase stage was demonstrated for all aging conditions which may come from the ejection of volatiles from “dangling” chains and/or small molecules (residual

monomers, absorbed water, and solvents), which coincides with GC/MS and mass-loss results. Subsequently, the T_g values increased regularly which indicates the decrease in molecular chain mobility induced by oxidation [45]. One of the first factors that come to mind is the crosslinking formed by the termination of two alkyl radicals. Another possibility may be the additional hydrogen bonding formation and promoted the steric effect by introducing C=O bonds. In order to argue that the predominant crosslinking in terms of macromolecular architecture, it is not sufficient to only confirm the T_g increase. As a supplemental study, the occurrence of the crosslinking process was tentatively verified by sol-gel analysis of the virgin/aged AUN for aged at 200 °C under air. For the soluble fraction (SF), the unaged AUN had a 7.2 % SF (corresponding to the initial mass-loss as shown in Fig. 3). Then, the SF dropped to almost zero (less than 0.5 %) after even a short time of thermal aging. In addition, a decrease of swelling degrees was demonstrated along with aging process, as shown in Fig. 5. This second result has two possible explanations: (i) the chemical changes occurring in AUN produce a lower affinity with the toluene used as the swelling solvent, or (ii) the crosslink density increases, reducing the swelling degree. Regardless, the most striking result is the absence of SF after thermal aging. If chain scission is favored compared with crosslinking, SF should increase along with the progress of oxidation as in the previous study of AUN oxidation [28]. Therefore, it would be reasonable to consider the “qualitative” predominant crosslinking by combining experimental results (swelling degree, SF, and T_g). In conclusion, the overall experimental results suggest in favor of the ejection of several structural units accompanied by crosslinking. Let us recall

that in tridmensionnal networks such as AUN system, number of elastically active chains increase by 2 for each crosslinking and decrease by 3 for each chain scission [24]. According to the abovementioned results, it possibly satisfies the 2(crosslinking) - 3(chain scission) > 0, i.e., the concentration in produced crosslinks exceeds 2/3 of chain scission ones.

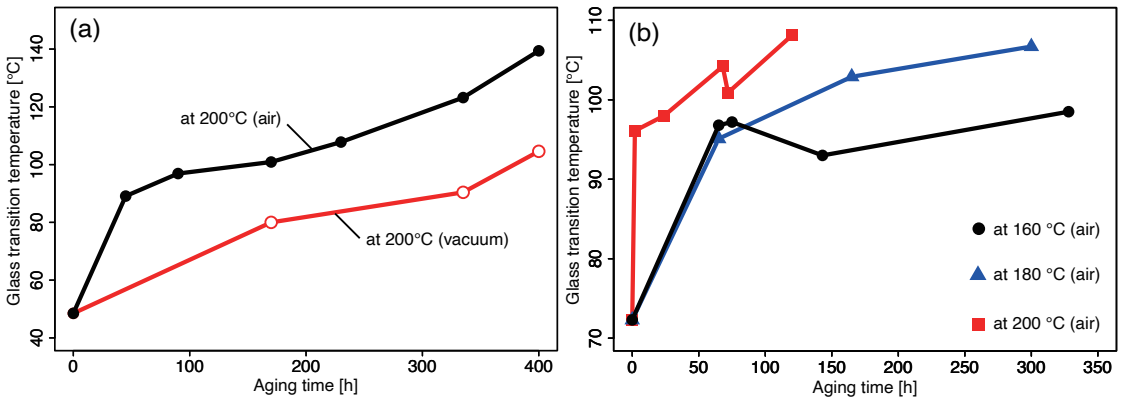


Fig. 4. Evolution of T_g under thermal aging: (a) comparison of T_g changes at 200 °C under air and vacuum conditions, as assessed by DSC; and (b) temperature dependence of T_g evolution, as assessed by DMA.

[(Color), (2-column fitting image)].

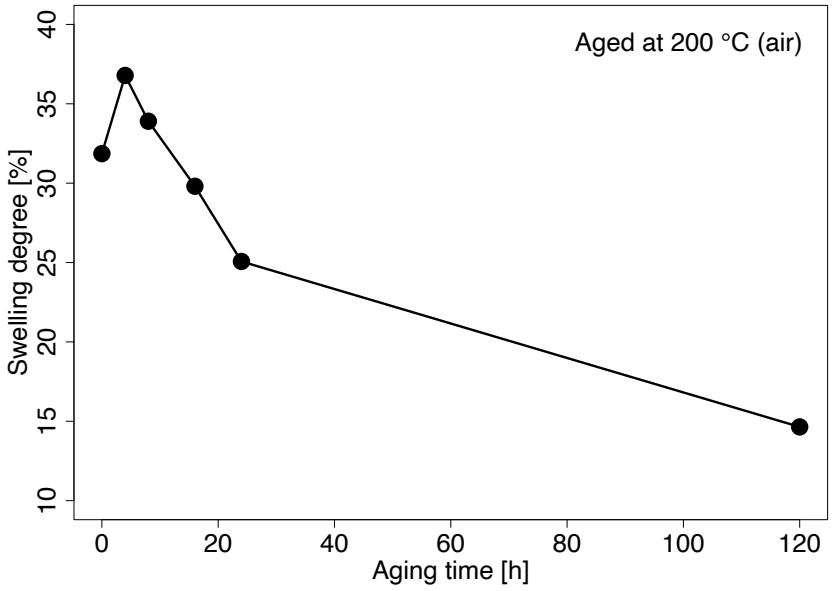


Fig. 5. Swelling degree of virgin/aged AUN at 200 °C under air.

[(1-column fitting image)].

3.3. Mechanical changes

The representative stress–strain curves for the virgin and aged AUN are shown in Fig. 6 (actual tensile tests were conducted five times per sample). In the virgin state, AUN displays slightly plastic behavior, because the sample displays a maximum stress for a strain of approximately 6%, and it fails at approximately 6.5%. Although aged samples display very minor changes to their elastic moduli, the plastic domain disappears and the samples fail in the elastic domain when severely aged. It is important to note that the area under the stress–strain curve regularly decreases compared with the virgin AUN for all aging conditions. This possibly implies embrittlement of the network structure because the sample toughness is sometimes used to describe the area under the stress–strain curve, as reported in Ref. [13]. The loss of

toughness is more significant in air aged AUN than aged under vacuum, which possibly originates from the restriction of molecular chain mobility arisen from the oxidation process. It is also important to note that the elastic modulus is not significantly changed for all temperatures under investigation (160, 180, and 200 °C), while it decreases by thermal aging at 200 °C under vacuum. This also relates to the cohesive energy density (CED) associated with the progress of oxidation [46]. These detailed mechanisms will be discussed in the Discussion section.

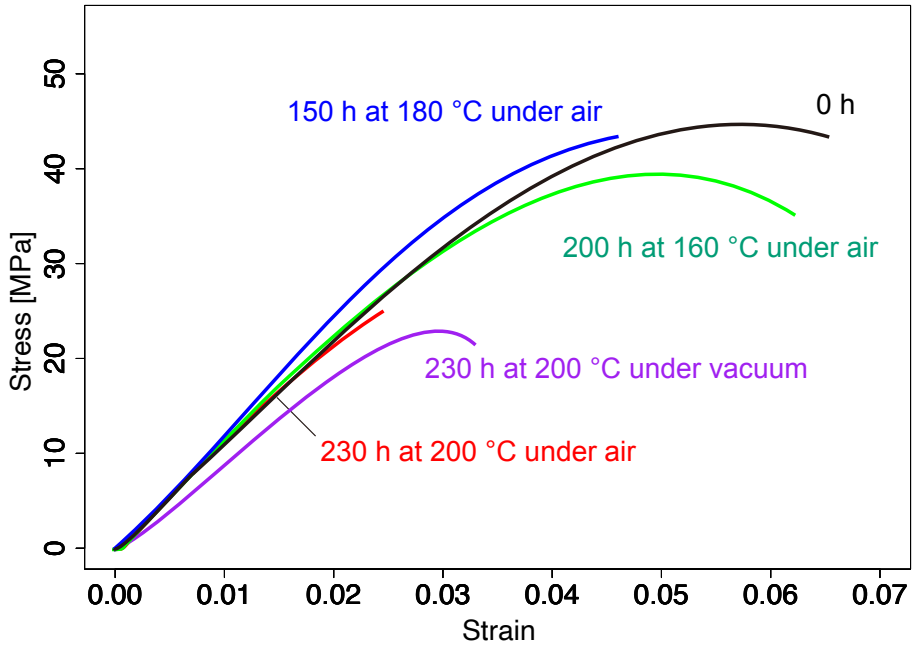


Fig. 6. Representative stress–strain curves for virgin/aged AUN.

[(Color), (1-column fitting image)].

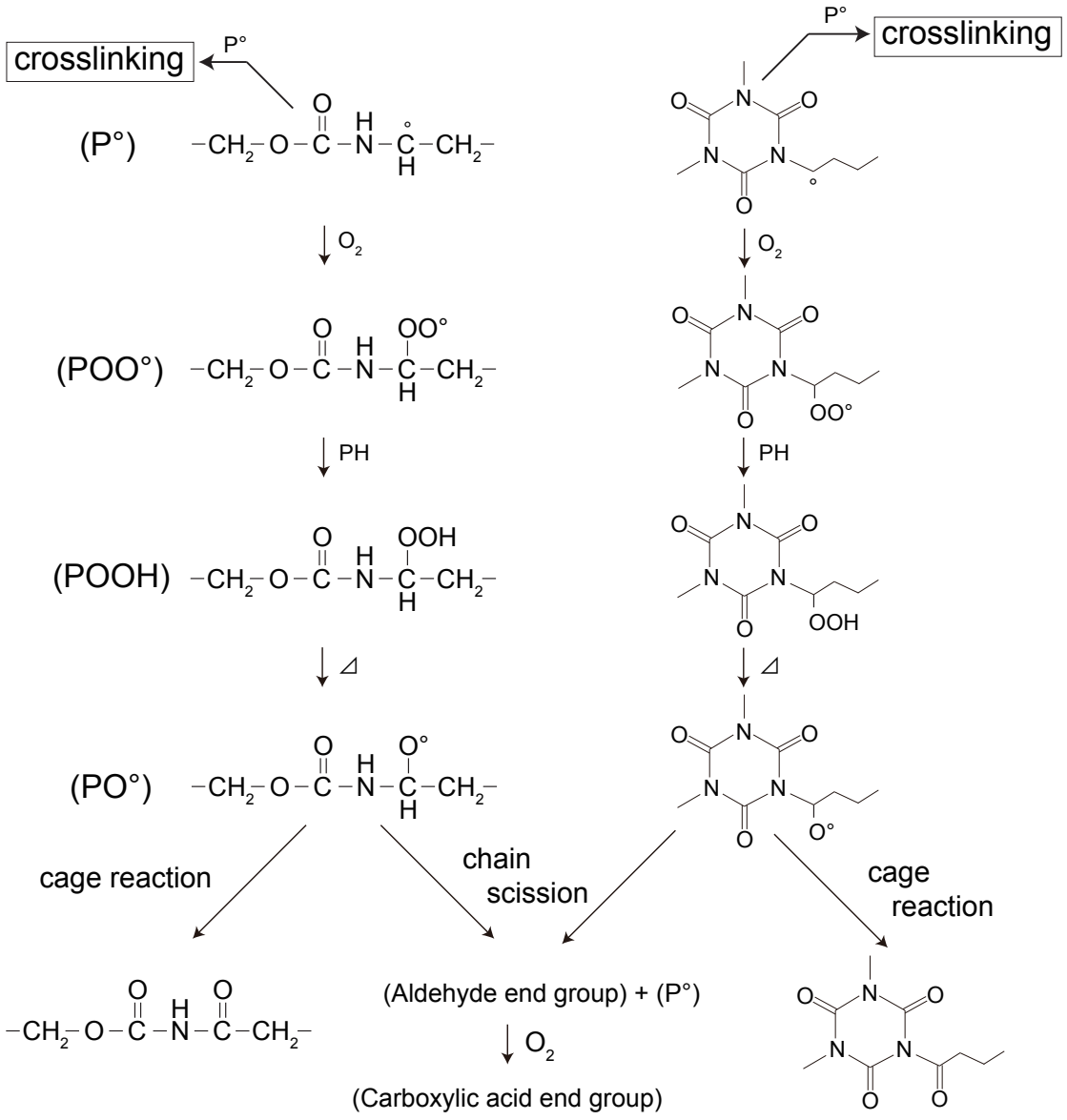
4. Discussion

In this section, based on the experimental results, we provide a coherent explanation of the AUN thermal aging mechanism. The main aims of this section are as follows:

- To propose a chemical mechanism for the thermal and thermal oxidative aging of AUN.
- To discuss the structural properties involved in the mechanical failure of AUN during thermal aging.
- To derive a novel kinetic model predicting the appearance of chemical markers relating to chemical aging effect.

4.1. Chemical mechanism

The main chemical marker associated with thermal oxidative aging is the appearance of carbonyl species (presumably imides), as observed by FTIR spectroscopy (Fig. 2). We stress that this marker is observed only in the presence of oxygen and therefore must correspond to an oxidation product. The most reasonable explanation for this is the oxidation of the two methylene groups in the α-position of heteroatoms in the system (i.e., urethane-linkage and isocyanurate ring). Here, we propose an oxidative degradation path from two reactive sites in the α-position of heteroatoms, as shown in Scheme 2.



Scheme 2. Proposed oxidation scheme of AUN thermo-oxidation.

[(2-column fitting image)].

According to our experimental results, only a limited number of chain scissions are possible (except for the chain scission from the "dangling chain," discussed later).

Expressed otherwise, alkoxy radicals can be converted into "chain" imides without requiring chain

scissions, which is consistent with the case of polyamides [19] and epoxies [47]. The chemical structure of "chain" imide in the AUN system corresponds to the N-acylurethane, which has the absorption band in the region of 1780-1765 cm^{-1} and at 3240 cm^{-1} (broad) [38]. Note that it does not contradict the fact the continuous development of the shoulder at 1770 cm^{-1} from the beginning of thermal aging, which could be the important indicator of AUN thermal aging (the absorbance at 1770 cm^{-1} is used to estimate the concentration of imide used in the kinetic model). The appearance of a small and broad absorption at 3240 cm^{-1} is also observed in severely aged AUN at 200 °C. A mechanistic scheme for polyamide 11 is presented in Ref. [19]; there, hydrogen abstraction was reported at the α-position of the amino group in the auto-oxidation process, and this reaction mechanism corresponded well with the photo-oxidation scheme in the acrylic-urethane system, as presented by Larché, Bussière, and Gardette [22]. In this work, the increase in absorbance at 1770 cm^{-1} is quite significant, while the development of the peak at 3240 cm^{-1} could not be seen as a remarkable peak. This may originate from two reasons: (i) the oxidation of CH_2 next to the isocyanurate ring can yield the imide structure without N-H bond (corresponding to the peak at 3240 cm^{-1}), as shown in Scheme. 2 (on the other hand, the oxidation of CH_2 next to the urethane group can form the imide structure with N-H bond), (ii) the molar absorptivity of N-H bond in the imide structure is smaller than the N-H bond in pristine urethane (Ref. [48,49]). As another oxidation route in Scheme. 2, carboxylic acid formation via chain scission may be possible, and the bands at 1756 cm^{-1} and 1711 cm^{-1} in the IR spectra were assigned to isolated carboxylic acid and non-isolated carboxylic acid [19,50]. In addition to

these bands, the non-negligible shoulder in our case was also formed in the domain 1800–1780 cm^{-1}, especially in the severely aged AUN sample, as shown in Fig. 2. The development of this domain may imply the accumulation of an oxidation product from acrylic-polyol. Lazzari and Chiantore [39] assumed that the CH_2 in the α-position of the ester group was the reactive site in the oxidation process and could form anhydrides and/or γ-lactones [39,40]. In the IR spectrum, the absorption bands at 1805 cm^{-1} and 1780 cm^{-1} can be attributed to anhydrides and γ-lactones, respectively. However, it is important to note that the BDE for the C–H bond at the α-position of the ester was theoretically estimated to be approximately 380–400–kJ mol^{-1} [51,52], significantly larger than the BDE at the α-position of an N atom (approximately 360 [$kJ \cdot mol^{-1}$]). Therefore, we assumed the radical attack of hydrogen abstraction to primarily occur at the C–H bond in the α-position of an N atom, rather than the CH_2 in the α-position of the ester group, owing to the difference in BDEs between the two reactive sites. Although the selective attack on the principal oxidation site (i.e., α-position of an N atom) could occur for the pristine AUN, the oxidation of the acrylic-polyol-part could be possibly caused after the depletion of the principal sites. This gradual mechanism may be the reason why oxidation of the polyol-part was suggested in the late stage of degradation. In addition, the decomposition of N-H groups (in urethane) and formation of aminyl radicals were also implied from FTIR spectroscopy (Fig.2). It is also needed to be considered for establishing a kinetic model of AUN thermal aging. According to the previous paper [53], the coupling of those two aminyl radicals can occur; in other words, the following mechanism would be envisaged: $N^{\circ} + N^{\circ} \rightarrow N - N$ (crosslink). According

to the abovementioned discussions, the first attempt at a kinetic model of AUN thermal aging is proposed in Section 4.3.

Next, let us consider the mechanisms of the increase in T_g (Fig. 4) from the theoretical equation governing the T_g change that considers the entropy of network polymers: the DiMarzio theory [65].

$$T_g = \frac{T_{gl}}{1 - K_{DM} n F}. \quad (4)$$

where T_{gl} is the glass transition temperature of the corresponding "virtual" linear polymer, K_{DM} is the DiMarzio's universal constant, n is the crosslink density, F is the flex parameter. The higher is F, the higher is the inertia of rotatable units, and the lower is the chain mobility. Compared with experimental results, the crosslink formation caused by oxidative degradation should contribute to the increase in T_g. It can yield through the coupling of two alkyl radicals, as demonstrated in Scheme. 2. As reported in Ref. [54], such alkyl radicals are created even under an inert atmosphere, possibly explaining why the T_g increased at 200 °C under vacuum conditions. However, the introduction of C=O groups on the molecular chain can also increase T_g through the increase T_{gl} and/or F in Eq. (4). The introduction of C=O groups possibly act as hydrogen bonding sites and enhance steric effects resulting in the increase of cohesive energy and reduction of molecular mobility, which relates with the T_{gl} and F, respectively [45,46]. Fig. 4(a) suggests that the increase in T_g under vacuum is somewhat mitigated compared to the thermal aging

1 under air. In addition to oxidative crosslinking, it can also be explained by the elimination of the effect of
2 the introduced C=O groups in vacuum. The initial rapid increase in T_g is also associated with the emission
3 of volatile components generated from the scission of several units (e.g., styrene and MMA) from "dangling"
4 chains of the acrylic linear component, which is consistent with mass loss (Fig. 3) and GC/MS results
5 (Table. 1). Since "dangling" chains can act as similar to "plasticizer" in the system, the loss of "dangling"
6 chains (ejection of several cleaved units from the acrylic linear part) might explain both the increase of T_g
7 and mass loss in aging process. As one of the supporting results of the mechanism, the ^{1}H-NMR spectra
8 change for thermally aged polyol (linear prepolymer) was studied (see Fig. S4 in the Supplementary
9 Materials). The results revealed that C=C bonds were not formed in thermally aged uncrosslinked acrylic
10 components at 200 °C under vacuum. If numerous random main chain scissions were present, C=C bonds
11 would be detected. Combining these results with those of the GC/MS analysis, we find support for our
12 claim that the scission and ejection of several structural units are implied by "dangling" chains (i.e., MMA
13 and St units located in chain ends).
14
15 4.2. End-of-life criteria
16 Here, we discuss the structural properties involved in the mechanical failure of the AUN during thermal
17 aging. From Fig. 6, we can summarize the notable features of these curves as follows:
18

- Modulus changes in the elastic region are not significant for all temperatures under investigation (160, 180, and 200 °C).
- The maximum elongation is decreased in the severely degraded case (i.e., embrittled), and the yield stress is also decreased when the sample is brittle.

Note that the tensile test was performed at room temperature, and the analyzed AUN is in the glass state. According to Ref. [55], the elastic modulus of a thermosetting polymer in the glassy state should be proportional to the cohesive energy density (CED). Although the oxidation of CH_2 groups at the α-position of an N atom can yield imide structures, we assume the effect on the CED possibly remains limited. As suggested by Van Krevelen (Ref. [46]), the CED can be estimated by the "additive group contribution method":

$$CED = \sqrt{\frac{\sum_i E_{coh}^{(i)}}{\sum_i V_m^{(i)}}} \tag{5}$$

where $E_{coh}^{(i)}$ is the cohesive energy of each group and $V_m^{(i)}$ is the molar volume of each group. The oxidation with the formation of the imide structure can increase both the denominator and the numerator, and their square root contributes to the CED. As a result, the CED of the network structure, which can contribute to the physical properties, may not change significantly by the progress of oxidation. In the

present system, the T_g increased, and the modulus did not change significantly along with the thermal oxidation, which the decrease in molecular chain mobility can justify due to crosslinking and/or hydrogen bonding formations. These results are not surprising case. In fact, it has been reported that in the case of an oxidized epoxy system, the change in CED was limited, and the rubbery modulus changed only slightly; however, the T_g increased significantly (Ref. [56]). On the other hand, the decrease of the elastic modulus in thermally aged samples under the inert condition could be explained that the contribution of chain-scission was only occurred without any oxidation. Concerning the second comment on the tensile characteristics, it suggests the significance of toughness as an indicator of the risk of mechanical failure, because toughness loss can be considered as an "embrittlement level." As stated in the Introduction section, toughness could be sometimes assessed from the area beneath the stress–strain curve, as described in [13]. In our study, the calculated toughness was markedly decreased by thermal aging for all temperature grades (see Fig. S5 in the Supplementary Materials). Here, we assessed the potential correlation between the toughness loss and the progress of thermal aging. Figure 7 plots toughness with respect to the concentration of the main chemical marker (i.e., imide) and the T_g values. These results present a strong linear correlation between the loss of toughness, accumulation of oxidized species, and T_g increase. As stated in Section 3.2, the increase in T_g should be related to the extent of crosslinking. As shown in Fig. 4(a), the AUN underwent significant crosslinking regardless of whether it was aged under air or vacuum conditions. However, the crosslinking efficiency was much higher when aged under air. Hence, the additional

1 likelihood of chemical and/or physical crosslinking (corresponding to the covalent bonds and inter-chain
2 hydrogen-bonding, respectively) may have arisen from oxidation. In addition, the toughness loss is
3 proportional to both the accumulation of imide and T_g values, as shown in Fig. 7. As a side note, the
4 influence on T_g and toughness from the oxidation of acrylic-part cannot be ruled out, as implied in FTIR
5 spectra (Fig. 2). Suppose we want to decouple the contribution of the urethane-part oxidation from the
6 linear-part oxidation. In that case, comparing oxidized urethane-networks crosslinked with several different
7 polyols (i.e., linear part) will be needed. It should be worth for further study to discuss the impact of liner-
8 part oxidation in a future publication. By the way, it should be noted that the imide accumulation, which
9 indicates the progress of chemical aging, is correlated with the amount of chemical and/or physical
10 crosslinking. Therefore, we can make rough predictions of service lifetime under arbitrary temperatures
11 using a kinetic model of AUN thermal degradation. In the next section, we establish a novel kinetic model
12 for thermal aging.
13

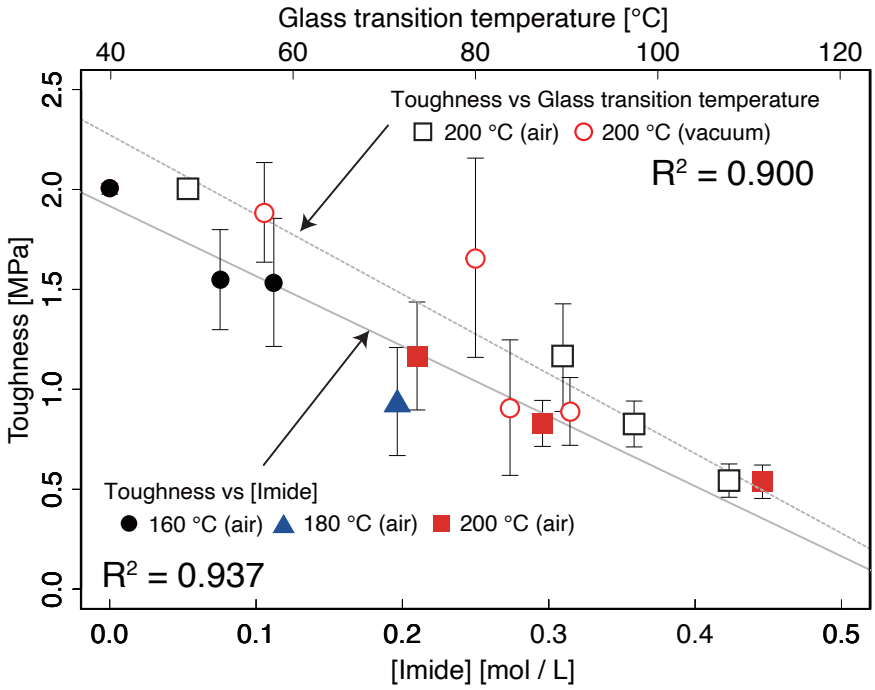


Fig. 7. Plot of toughness vs. the concentration of imide (lower) and T_g values (upper) before/after AUN aging under air/vacuum (solid line and solid dot line denote linear fit regression of toughness vs [Imide] and toughness vs glass transition temperature, respectively).

[(Color), (1-column fitting image)].

4.3. Kinetic modeling of AUN degradation

Here, we attempt to establish a kinetic model for AUN thermal oxidation from the experimental results. As previously mentioned, one purpose of the model is to simulate the imide build-up behavior as the primary marker of the chemical aging effect. Then, we consider the mechanically valid scheme for AUN oxidation, including a reaction path yielding imide species via a cage radical mechanism. First, the decomposition of hydroperoxide (denoted as $POOH$) can be described by the following reaction steps:

$$POOH \rightarrow PO^{\circ} + HO^{\circ},$$

$$(PO^{\circ} + HO^{\circ})_{cage} \rightarrow \text{imide} + \mathrm{H_2O}, \qquad (\gamma_1)$$

$$PO^{\circ} + PH \rightarrow \text{end chain imide} + P^{\circ} + \text{chain scission}, \qquad (\gamma_2)$$

$$PO^{\circ} + PH \rightarrow \text{Hydroxyurethane } (-O - CO - NH - CHOH - CH_2 -) + P^{\circ} \qquad (\gamma_3)$$

$$+ \text{chain scission},$$

$$HO^{\circ} + PH \rightarrow P^{\circ} + \mathrm{H_2O}, \qquad (1 - \gamma_1)$$

where γ_1, γ_2, and γ_3 are the yields of the corresponding reaction paths; they satisfy $\gamma_1 + \gamma_2 + \gamma_3 = 1$. Hydroxyurethane should destabilize and be converted into carboxylic acid via chain scission [27]; this is expressed as

$$\text{Hydroxyurethane} \rightarrow \text{Carboxylic acid} + \text{chain scission}.$$

Next, the creation of alkyl radicals and subsequent crosslinking was experimentally indicated, even during thermal aging under vacuum conditions. Hence, an extra path for thermolytic alkyl radical formation must be considered:

$$PH \rightarrow P°.$$

Here, PH denotes the polymer substrate (here, C–H bonds at the α-position of an N atom).

According to Fig. 2, the loss of N-H group was observed for all aging conditions under air (200 °C, 180 °C, and 160 °C). Thus, we introduced the probable paths of oxidative decomposition of N-H bonds [57] as follows:

$$NH + POO° \rightarrow N° + POOH\,,$$

Here, NH and $N°$ denotes the N–H bonds in the urethane-linkage and the aminyl radical (as shown in Scheme. 1(c)), respectively. According to the previous work [53], the bimolecular association of two aminyl radicals can occur and yield a crosslink as follows:

$$N° + N° \rightarrow N - N,$$

In case of aminyl radicals, hydrogen abstraction and β-scission are rarely occurred as reported by Ogawa and Nomura [58]. The nitroxide radicals ($NO°$) could be formed through the propagation of aminyl radicals,

likewise stabilizers of the amine family. Although $NO°$ can act as stabilizers by scavenging alkyl radicals, the stabilizing mechanism is assumed to be negligible because the efficiency of the stabilization effect is quite limited at high temperature (typically $T \geq 150$ °C) [57].

Lastly, the formation of a peroxide-type product ($POOP$) can be assumed in termination processes (i.e., coupling of $P° + POO°$ and $POO° + POO°$). It has been previously suggested that the decomposition of $POOP$ generates imides and carboxylic acids in equal proportions [19,27]. By summarizing the discussions so far, the overall mechanism of AUN oxidation is proposed as follows:

$$PH \rightarrow P°, \qquad (k_t)$$

$$POOH \rightarrow (\gamma_1 + \gamma_2)\,\text{Imide} + 2(\gamma_2 + \gamma_3)P° + \gamma_3\text{Hydroxyurethane} + \gamma_2 S, \qquad (k_1)$$

$$P° + O_2 \rightarrow POO°, \qquad (k_2)$$

$$POO° + PH \rightarrow POOH + P°, \qquad (k_3)$$

$$NH + POO° \rightarrow N° + POOH, \qquad (k_{NH})$$

$$P° + P° \rightarrow X, \qquad (k_4)$$

$$N° + N° \rightarrow X, \qquad (k_N)$$

$$P° + POO° \rightarrow POOP, \qquad (k_5)$$

$$POO° + POO° \rightarrow POOP + O_2, \qquad (k_6)$$

$$POOP \rightarrow \text{Imide} + \text{Hydroxyurethane}, \qquad (k_{1d} \sim k_1)$$

$$\text{Hydroxyurethane} \rightarrow \text{Carboxylic acid} + S, \qquad (k_d)$$

where S and X denote chain scissions and crosslinking, respectively. k_i is the rate constant for each reaction considered.

The formulas of corresponding differential equation system are presented in the Supplementary Materials. We here describe the method for determining the rate constants (k_i) of each reaction process used in the kinetic model on AUN oxidation. It should be noted that the parameter configuration is basically referring to the previously developed kinetic models of polyamide 11 [27] and epoxy/amine [14] systems with similar chemical structures (in terms of the common features of oxidation mechanisms). Firstly, the rate constants concerning propagation steps (k_2, k_3) are fixed from a priori based on literature [14,27,59], since the radical propagation process is known to exhibit common characteristics regardless of the type of polymer (see, e.g., Refs. [18,26,27,31,60]). k_2 is the rate constant of oxygen added to $P°$; it is assumed to be significantly rapid in comparison with k_1 and k_3. Here, k_2 is taken as 10^6 [L mol^{-1} s^{-1}] without temperature dependence (i.e., $E_2 = 0$), which has been validated in polyamide and epoxy/amine systems [14,27]. In addition, k_3 corresponds to the radical propagation process of hydrogen abstraction by $POO°$ radicals. Conventionally, k_3 values, including its temperature dependence, are determined by Korcek's law [59] according to the dissociation energy values for the C–H bond (BDE) of the considered oxidative site. Hence, we assume that the selective attack of hydrogen abstraction occurred primarily at the C–H bond in the α-

position of an N atom, because the BDE here should be considerably smaller (360 kJ·mol^{-1}) than the olefinic BDE (390–395 kJ·mol^{-1}) [31], expressed as

$$k_3 = \exp\left(19.517 - \frac{55000}{RT}\right), \quad (6)$$

where R is the gas constant (kJ mol^{-1} K^{-1}) and T is the absolute temperature [K]. Secondly, we assume the radical termination steps (k_4, k_5, k_6, and k_N) are basically performed quickly due to the samples aged at high-temperature environments; hence, they could be assumed to be virtually temperature independent (i.e., $E_4 = E_5 = E_N = 0$). In general, the termination steps should depend on the molecular mobility, and previous studies [31] have shown that the $POO° + POO°$ termination has a minimal temperature dependence ($E_6 =$ 0-10 [kJ·mol^{-1}]) because it is expected to have smaller molecular mobility than the other termination steps (steric effect). Lastly, the initiation rate constant (k_1) corresponds to the event of $POOH$ decomposition. Since the stability of $POOH$ depends on the chemical nature of target systems, k_1 is treated as a fitting parameter in this study. In addition, the rate constant for $POOP$ unimolecular decomposition should be slightly smaller than (but very close to) the value for $POOH$ decomposition found in Sagar's work [61]. Thus, we provisionally assume that $k_{1d} \sim k_1$. The other rate constants (k_t, k_1, k_{NH}, k_4, k_N, k_5, k_6 and k_d) vary from system to system according to several factors (e.g., chemical nature and molecular mobility); these parameters are needed to be obtained by a trial-and-error process. Starting

from a set of parameters from existing models [14,27] that have been used successfully, we first determined the main rate constants ($k_1, k_4, k_5,$ and k_6) in the auto-oxidation loop to fit our data (the change in concentration of imide, PH, and NH) and not violate the physically realistic hierarchy ($k_4 > k_5 > k_6 > k_2 \gg k_3$). After these parameters (for the radical initiation, propagation, and termination steps) have been completely fixed, the other minor parameters ($k_t, k_d, k_N,$ and k_{NH}) were determined by setting their initial values to 0 and adjusting them manually little by little. In this study, the change in oxygen concentration and the effects of the oxygen profile are neglected because the thin film was subjected to thermal aging (i.e., non-DLO conditions).

The set of differential equations were numerically solved using the MatLab® ode23s solver. The following initial conditions were used as input data:

$[PH]_0 = 1.0$ [mol L^{-1}], $[NH]_0 = 0.5$ [mol L^{-1}], $[POOH]_0 = 0.01$ [mol L^{-1}], $[O_2] = 4 \times 10^{-4}$ [mol L^{-1}], $[P^\circ]_0 = [POO^\circ]_0 = [POOP]_0 = [Imide]_0 = [\text{Carboxylic acid}]_0 = [\text{Hydroxyurethane}]_0 = X_0 = S_0 = 0$.

The initial concentration of the polymer substrate $[PH]_0$ corresponding to the C–H bond concentration in the α-position of an N atom can be calculated from the sample composition, as shown in Section 2.1. $[NH]_0$ corresponding to the initial concentration of N-H bond in this system can be also estimated in the same manner as $[PH]_0$. Time-dependent $[PH]$ and $[NH]$ (test data) are calculated from the absorbances

of corresponding chemical species in FTIR spectra as the relative decrease from the initial concentration of $[PH]_0$ and $[NH]_0$.

$$[X] = \frac{\mathrm{Abs}(t)}{\mathrm{Abs}(t=0)}[X]_0 \qquad (X = NH \text{ or } PH) \tag{7}$$

where $\mathrm{Abs}(t)$ is the time-dependent specific absorption in FTIR spectra. To estimate the relative changes in $[PH]$ and $[NH]$, we used the shoulder of the C–H region at 2859 cm^{-1} and the bands at 3385 cm^{-1}, which are attributed to the C–H bonds at the α-position of the urethane groups and the N–H stretching vibration (in urethane). In addition, $[O_2] = 4 \times 10^{-4}$ suggests a coefficient of O_2 solubility of ~ 10^{-8} [mol L^{-1} Pa^{-1}], by considering Henry's law under the oxygen partial pressure (0.21 bar; ambient air). The order of magnitude of O_2 solubility does not contradict the O_2 solubility of polyurethane rubber reported in Ref. [62].

The output data described the concentration of the following series of reactive species: $[P°], [POO°], [POOH], [POOP] \cdots$. The best-fitting rate constants (k_t, k_1, k_{NH}, k_4, k_N, k_5, k_6, γ_1, γ_2 and γ_3) are determined by considering compatibility with the experimental results, as shown in Fig. 8. The concentration of imide was estimated using Lambert–Beer's law [Eq. (1)]. The obtained set of rate constants are presented in Table. 2, and γ_1, γ_2, and γ_3 are listed in Table 3.

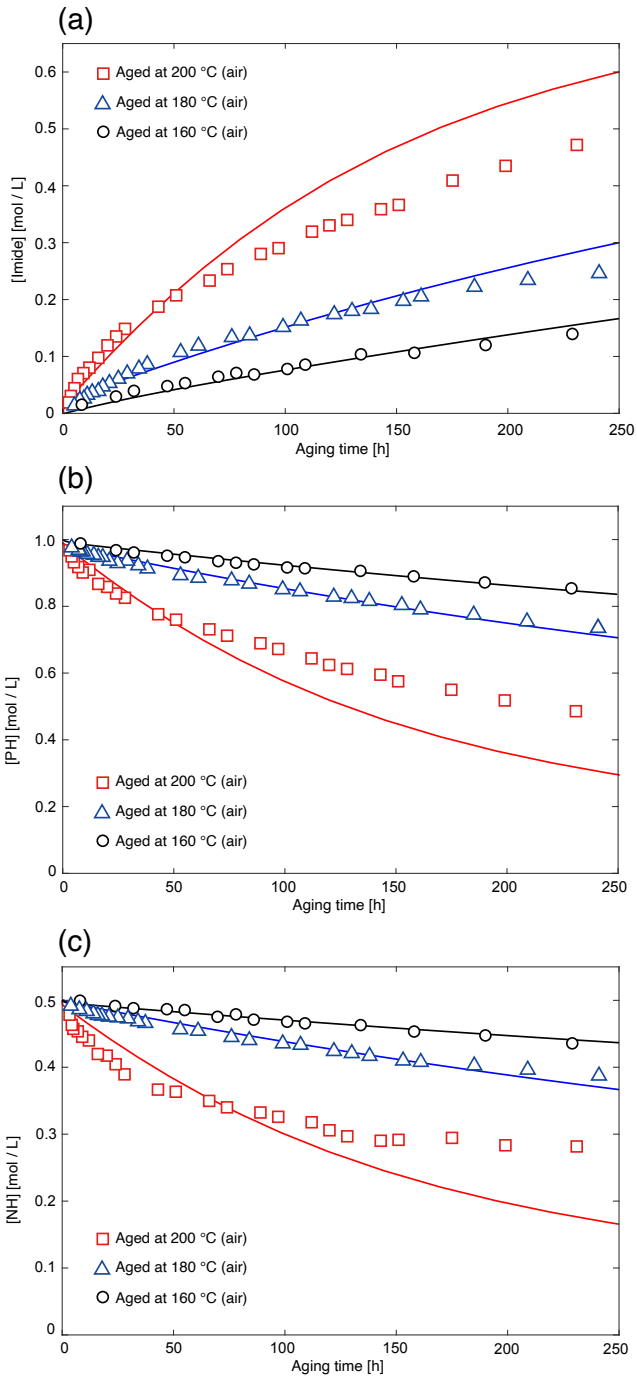


Fig. 8. Changes with respect to aging time in the concentration of (a) imide, (b) PH, and (c) NH between 160 °C and 200 °C. The simulation curves and experimental data are presented as solid lines and open symbols, respectively.

[(Color), (1-column fitting image)].

Table 2. Rate constants and activation energies (E_a) used for the simulation and determined by the numerical reverse method at 160 °C.

Rate constants	k_t	k_1	k_2	k_3	k_{NH}	k_4	k_N	k_5	k_6	k_d
[mol L^{-1} s^{-1}]	10^{-10}	3×10^{-5}	10^6	69.7	28	9.6×10^{10}	10^{10}	5.85×10^9	1.6×10^9	10^{-7}
E_a [kJ mol^{-1}]	155	195	0	55	34.2	0	0	0	3.8	0

Table 3. Yields of the initiation process, determined by the numerical reverse method.

γ_1	γ_2	γ_3
0.78	0.15	0.07

The results suggest the following comments:

- At low conversion (i.e., [PH] > 0.7 [mol L^{-1}], [imide] < 2.0 [mol L^{-1}]), the validity of the simulation with imide build-up, PH and NH depletion is confirmed.
- The simulation between 180 °C and 200 °C overestimated oxidation progress at high conversion. It possibly caused by the sensitivity loss of experimental data responsible for volatilized products (as shown in Fig. 3) and/or compensated by the oxidation of CH_2 in the α-position of the ester (so-called "co-oxidation" might coexist) [60].
- The simulation results are sensitive to the k_1 values for the initiation step, which reflect the reactivity

of the AUN system (i.e., stability of $POOH$). We additionally conducted the sensitivity analysis of the simulation results to the variation in k_1 values (see Fig. S6 in the Supplementary Materials).

Table. 4 compares the obtained initiation rate constant k_1, initial $POOH$ concentration $[POOH]_0$, and carbonyl species yield obtained for each $POOH$ decomposition event for polyamide 11 [27] and epoxies [14]. The fitted k_1 value was lower than the other cases, which may reflect the difference in $POOH$ stability. The assumed $[POOH]_0$ appears acceptable because it is comparable to previously successful models. In this case, the imide yield for each $POOH$ decomposition event was 0.78; that is, 78% of $POOH$ yielded imide. This was comparable with the case of polyamide 11 and lower than that of epoxies.

Table 4. Comparison of k_1 at 160 °C, $[POOH]_0$, and the carbonyl species yields for each $POOH$ decomposition event (denoted as γ) against the values obtained in previous works. The k_1 values were extrapolated by the corresponding activation energy for cases of polyamide 11 and epoxies.

Sample	k_1 at 160 °C (s^{-1})	$[POOH]_0$ (L mol^{-1})	γ
AUN (present work)	3.00×10^{-5}	1.0×10^{-2}	0.78
Polyamide 11 [27]	3.76×10^{-3}	3.0×10^{-2}	0.77
Epoxies [14]	1.721×10^{-3}	1.0×10^{-3}	1.00

In addition, a simulation of the macromolecular architecture changes is discussed. The experimental characterization of the aged samples implies the predominance of chemical and/or physical crosslinking except for 160 °C, as discussed in Section 3.2. From the experimental results in this study, the number of chain scission is possibly limited, and the thermal oxidation scheme (Scheme. 2) suggests the crosslink formation by coupling alkyl radicals ($P°$). It is reasonable that the concentration in elastically active chains could be increased consistently under the increase in T_g for thermal aging. According to Refs. [15,63], the time-derivative of the concentration in elastically active chains corresponds to $2X - 3S$. The simulations in this work indicate that $2X - 3S$ remained positive for all aging conditions studied, even under vacuum conditions. In the case of 200 °C aging, $2X - 3S$ was larger under air than under vacuum conditions, as shown in Fig. 9; this is consistent with the evolution of T_g [Fig. 4 (a)]. It was found that $2X > 3S$ for all aging conditions provided $\gamma_2 < 0.27$. Here, the kinetic model was constructed under the (simplified) condition of $2X - 3S > 0,$ which is required by the "qualitative" extensive crosslinking inferred from the experimental results. It is required to carry out the continuous and intermittent stress-relaxation test to quantify the rate of crosslinking/scission accurately, submitted by Nichols and Gerlock [64]. Further upgrading the model using this method will be a worth for future works.

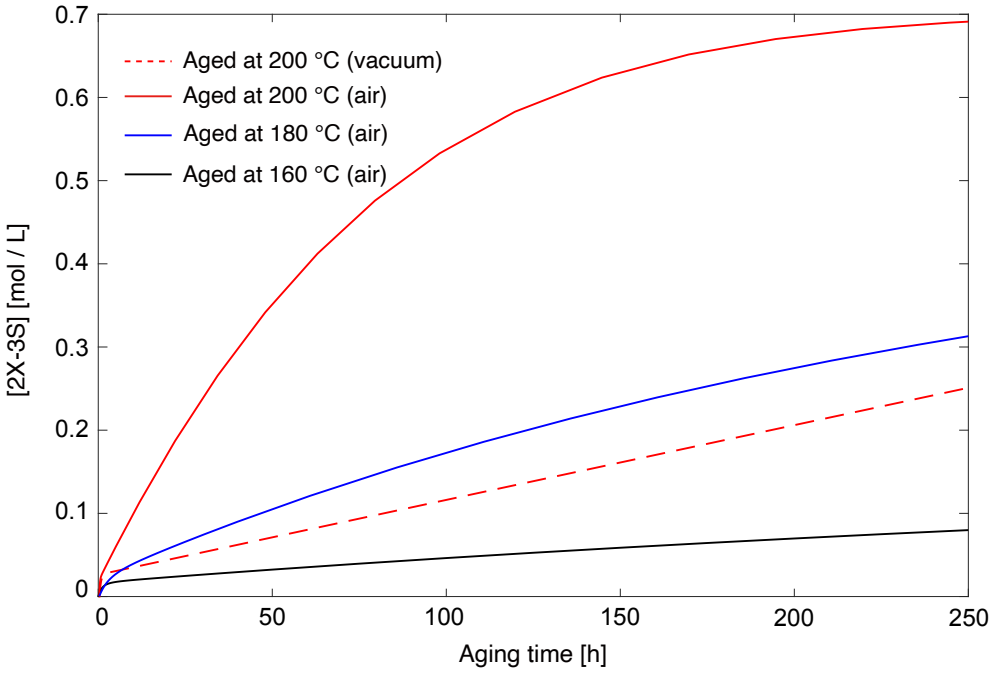


Fig. 9. Simulation of the changes in the concentration of $[2X - 3S]$ under air (at 160 °C, 180 °C, and 200 °C) and vacuum (at 200 °C) conditions.

[(Color), (1-column fitting image)].

Finally, the possibility of oxidation of CH_2 in the α-position of the ester in the acrylic-polyol component was actually implied, as discussed in Section 4.1. The oxidation of CH_2 in the α-position of the ester may need to be considered to improve the accuracy of our model at high conversion regimes when the principal oxidative site (i.e., the CH_2 in the α-position of heteroatoms) is exhausted. To improve our novel kinetic model, the so-called "co-oxidation model" might be employed in future work to consider more than two reactive sites, thereby establishing a more sophisticated kinetic model of AUN oxidation and improving

predictions of crosslinking and chain scission concentration [60]. In addition, extensive crosslinking was reported in the case of AUN "photo-aging" in our previous work [23]. The macromolecular change behavior of AUN exhibits common features between thermal and photo-aging cases. Hence, the possibility of extrapolating the established model for photo-oxidation phenomena is worth further research.

5. Conclusion

In this paper, the thermal aging of AUN was discussed by comprehensive characterization (FTIR, classical tensile experiment, DMA, sol-gel analysis, DSC, and GC/MS analysis). First, the analysis of chemical modifications arising from the aging process suggested the oxidization of CH_2 in the α-position of an N atom and the volatilization release of MMA and styrenic units from acrylic-polyol, which is responsible for mass loss from the AUN system. Based on the chemical scale discussions, a possible thermal aging scheme including a reaction path yielding "chain" imide via a cage radical mechanism was proposed, in accordance with previous research (i.e., thermo-oxidation of polyamides and AUN photo-oxidation). Another oxidation route corresponds to the conventional closed-loop scheme, which generates carboxylic acids via chain scission.

Next, macromolecular changes under thermal aging were studied, primarily from the evolution of the T_g values. In this work, the T_g values were gradually increased for all aging conditions (even at 200 °C under vacuum), which may indicate the predominance of chemical and/or physical crosslinking

(corresponding to the covalent bonds and inter-chain hydrogen-bonding, respectively), as confirmed by the absence of a soluble fraction and by the sol-gel analysis. A loss of toughness was also observed alongside the increase in T_g. Toughness can represent an important indicator of the risk of material failure (cracking), because toughness loss might be considered as an "embrittlement level." The toughness loss exhibited a strong linear correlation with the accumulation of the main oxidized product (i.e., imide) and the increase in T_g linked to aging-induced crosslinking. Using these correlations, we might make rough predictions of service lifetime using the kinetic model of the AUN thermal degradation, which can successfully reproduce the build-up of imide.

Finally, a first attempt at such a kinetic model of AUN thermal aging was proposed, based on mechanistic discussions derived from the analysis of chemical-scale discussions in the aging process. This was based on a model previously established for polyamide 11, with extra paths of thermolytic alkyl radical formation, oxidative N-H bonds decomposition and coupling of aminyl radicals. The validity of the simulation with imide build-up, PH and NH depletion was confirmed at low conversion. In addition, the predominance of crosslinking during thermal aging could also be reproduced. Our proposing kinetic model is not currently perfect, however, it is possibly acceptable for "mild" thermal aging (at low conversion). As one option for improving our kinetic model, the oxidation of acrylic-polyol may need to be considered. For the unaged system, the probability of oxidation at α-position of an ester group in acrylic-polyol can be estimated to be less than 0.1% at most based on the difference in BDEs between the

C–H bond α-position of an N atom and the α-position of an ester group. If the principal oxidation site (PH) is much exhausted, we should envisage the additional oxidation at α-position of an ester group in acrylic-polyol to obtain better prediction even at high conversion. Therefore, proposing a "full" kinetic model of AUN, which takes into account the specificities of linear polymer, would be worthwhile future research, and we believe that a kinetic model for pure thermal aging would help establish a kinetic model of AUN photothermal aging.

Acknowledgments

This work was supported by a Grant-in-Aid for JSPS (Japan Society for the Promotion of Science) Fellows (Number 19J20126). The authors gratefully acknowledge the Overseas Challenge Program for Young Researchers provided by JSPS for its financial support to living allowance and roundtrip fee.

Funding sources

This work was supported by Grant-in-Aid for JSPS (Japan Society for the Promotion of Science) Fellows (Number 19J20126).

References

[1] H.M.C.C. Somarathna, S.N. Raman, D. Mohotti, A.A. Mutalib, K.H. Badri, The use of

polyurethane for structural and infrastructural engineering applications: A state-of-the-art review, Constr. Build. Mater. 190 (2018) 995–1014. https://doi.org/https://doi.org/10.1016/j.conbuildmat.2018.09.166.

[2] A. Colin, M. Baba, P.-O. Bussiere, E. Cavaletti, F. Nizeyimana, S. Therias, Investigation of the thermo-oxidation mechanism of acrylic-urethane-silicone/amino-silane based topcoat, Polym. Degrad. Stab. 114 (2015) 115–124. https://doi.org/https://doi.org/10.1016/j.polymdegradstab.2014.12.011.

[3] D. Rosu, L. Rosu, C.N. Cascaval, IR-change and yellowing of polyurethane as a result of UV irradiation, Polym. Degrad. Stab. 94 (2009) 591–596. https://doi.org/https://doi.org/10.1016/j.polymdegradstab.2009.01.013.

[4] A. Bardin, P.-Y. Le Gac, S. Cérantola, G. Simon, H. Bindi, B. Fayolle, Hydrolytic kinetic model predicting embrittlement in thermoplastic elastomers, Polym. Degrad. Stab. 171 (2020) 109002. https://doi.org/https://doi.org/10.1016/j.polymdegradstab.2019.109002.

[5] J.-F. Larché, P.-O. Bussière, S. Thérias, J.-L. Gardette, Photooxidation of polymers: Relating material properties to chemical changes, Polym. Degrad. Stab. 97 (2012) 25–34. https://doi.org/https://doi.org/10.1016/j.polymdegradstab.2011.10.020.

[6] M.D. Failla, A. Brandolin, C. Sarmoria, E.M. Vallés, The effect of oxygen on the irradiation process of ethylene–butene copolymer, Polym. Degrad. Stab. 97 (2012) 1485–1494.

https://doi.org/https://doi.org/10.1016/j.polymdegradstab.2012.05.004.

[7] G. Oertel, PolyurethaneHandbook, MacmillanPublishingCo., NewYork, 1985.

[8] G. Li, B. Yang, C. Guo, J. Du, X. Wu, Time dependence and service life prediction of chloride resistance of concrete coatings, Constr. Build. Mater. 83 (2015) 19–25. https://doi.org/https://doi.org/10.1016/j.conbuildmat.2015.03.003.

[9] J.-F. Larché, P.-O. Bussière, J.-L. Gardette, How to reveal latent degradation of coatings provoked by UV-light, Polym. Degrad. Stab. 95 (2010) 1810–1817. https://doi.org/https://doi.org/10.1016/j.polymdegradstab.2010.05.005.

[10] J.F. Rabek, Photodegradation of Polymers, New York, 1996.

[11] B. Fayolle, L. Audouin, J. Verdu, Initial steps and embrittlement in the thermal oxidation of stabilised polypropylene films, Polym. Degrad. Stab. 75 (2002) 123–129. https://doi.org/https://doi.org/10.1016/S0141-3910(01)00211-7.

[12] A. David, J. Huang, E. Richaud, P. Yves Le Gac, Impact of thermal oxidation on mechanical behavior of polydicylopentadiene: Case of non-diffusion limited oxidation, Polym. Degrad. Stab. 179 (2020) 109294. https://doi.org/https://doi.org/10.1016/j.polymdegradstab.2020.109294.

[13] F. Dong, S. Maganty, S.J. Meschter, J. Cho, Effects of curing conditions on structural evolution and mechanical properties of UV-curable polyurethane acrylate coatings, Prog. Org. Coatings. 114 (2018) 58–67. https://doi.org/https://doi.org/10.1016/j.porgcoat.2017.09.018.

[14] E. Ernault, J. Dirrenberger, E. Richaud, B. Fayolle, Prediction of stress induced by heterogeneous oxidation: Case of epoxy/amine networks, Polym. Degrad. Stab. 162 (2019) 112–121. https://doi.org/https://doi.org/10.1016/j.polymdegradstab.2019.02.019.

[15] E. Richaud, P. Gilormini, M. Coquillat, J. Verdu, Crosslink Density Changes during the Hydrolysis of Tridimensional Polyesters, Macromol. Theory Simulations. 23 (2014) 320–330. https://doi.org/https://doi.org/10.1002/mats.201300143.

[16] R. Narayan, D.K. Chattopadhyay, B. Sreedhar, K.V.S.N. Raju, N.N. Mallikarjuna, T.M. Aminabhavi, Degradation profiles of polyester–urethane (hydroxylated polyester/diphenylmethane diisocyanate) and polyester–melamine (hydroxylated polyester/hexamethoxymethylmelamine) coatings: An accelerated weathering study, J. Appl. Polym. Sci. 97 (2005) 1069–1081. https://doi.org/https://doi.org/10.1002/app.21568.

[17] C.M. Seubert, M.E. Nichols, V.A. Cooper, J.L. Gerlock, The long-term weathering behavior of UV curable clearcoats: I. Bulk chemical and physical analysis, Polym. Degrad. Stab. 81 (2003) 103–115. https://doi.org/https://doi.org/10.1016/S0141-3910(03)00079-X.

[18] X. Colin, J. Verdu, Strategy for studying thermal oxidation of organic matrix composites, Compos. Sci. Technol. 65 (2005) 411–419. https://doi.org/https://doi.org/10.1016/j.compscitech.2004.09.011.

[19] O. Okamba-Diogo, E. Richaud, J. Verdu, F. Fernagut, J. Guilment, B. Fayolle, Molecular and

macromolecular structure changes in polyamide 11 during thermal oxidation, Polym. Degrad. Stab. 108 (2014) 123–132. https://doi.org/https://doi.org/10.1016/j.polymdegradstab.2014.05.028.

[20] M.M. Horikx, Chain scissions in a polymer network, J. Polym. Sci. 19 (1956) 445–454. https://doi.org/https://doi.org/10.1002/pol.1956.120199305.

[21] C. Sarmoria, E. Vallés, Model for a scission-crosslinking process with both H and Y crosslinks, Polymer (Guildf). 45 (2004) 5661–5669. https://doi.org/https://doi.org/10.1016/j.polymer.2004.06.006.

[22] J.-F. Larché, P.-O. Bussière, J.-L. Gardette, Photo-oxidation of acrylic-urethane thermoset networks. Relating materials properties to changes of chemical structure, Polym. Degrad. Stab. 96 (2011) 1438–1444. https://doi.org/https://doi.org/10.1016/j.polymdegradstab.2011.05.011.

[23] T. Ishida, R. Kitagaki, S. Yamane, H. Hagihara, Temperature dependence of structural alteration by ultraviolet irradiation in acrylic-urethane coatings studied by positron annihilation spectroscopy and solvent swelling behavior, Polym. Degrad. Stab. 162 (2019) 85–93. https://doi.org/10.1016/J.POLYMDEGRADSTAB.2019.02.007.

[24] T. Ishida, R. Kitagaki, H. Hagihara, Y. Elakneswaran, Challenges in prediction of significant structural changes during photochemical “degelation” of acrylic-urethane network, Polymer (Guildf). 186 (2020) 122035. https://doi.org/https://doi.org/10.1016/j.polymer.2019.122035.

[25] T. Ishida, R. Kitagaki, R. Watanabe, H. Hagihara, Y. Elakneswaran, H. Shinzawa, A study of

molecular architectural dynamics of crosslinked urethane during photo-aging by two-dimensional infrared correlation spectroscopy, Polym. Degrad. Stab. 179 (2020) 109242. https://doi.org/https://doi.org/10.1016/j.polymdegradstab.2020.109242.

[26] A. François-Heude, E. Richaud, E. Desnoux, X. Colin, A general kinetic model for the photothermal oxidation of polypropylene, J. Photochem. Photobiol. A Chem. 296 (2015) 48–65. https://doi.org/https://doi.org/10.1016/j.jphotochem.2014.08.015.

[27] O. Okamba-Diogo, E. Richaud, J. Verdu, F. Fernagut, J. Guilment, B. Fayolle, Molecular and macromolecular structure changes in polyamide 11 during thermal oxidation – Kinetic modeling, Polym. Degrad. Stab. 120 (2015) 76–87. https://doi.org/https://doi.org/10.1016/j.polymdegradstab.2015.06.005.

[28] T. Ishida, R. Kitagaki, H. Hagihara, Y. Elakneswaran, Role of moisture in photo-ageing - macromolecular architecture evolution of acrylic-urethane network, Polym. Test. 96 (2021) 107123. https://doi.org/https://doi.org/10.1016/j.polymertesting.2021.107123.

[29] P. Gijsman, W. Dong, A. Quintana, M. Celina, Influence of temperature and stabilization on oxygen diffusion limited oxidation profiles of polyamide 6, Polym. Degrad. Stab. 130 (2016) 83–96. https://doi.org/https://doi.org/10.1016/j.polymdegradstab.2016.05.024.

[30] A. Quintana, M.C. Celina, Overview of DLO modeling and approaches to predict heterogeneous oxidative polymer degradation, Polym. Degrad. Stab. 149 (2018) 173–191.

https://doi.org/https://doi.org/10.1016/j.polymdegradstab.2017.11.014.

[31] E. Richaud, O. Okamba Diogo, B. Fayolle, J. Verdu, J. Guilment, F. Fernagut, Review: Auto-oxidation of aliphatic polyamides, Polym. Degrad. Stab. 98 (2013) 1929–1939. https://doi.org/https://doi.org/10.1016/j.polymdegradstab.2013.04.012.

[32] K.J. Voorhees, F.D. Hileman, I.N. Einhorn, J.H. Futrell, An investigation of the thermolysis mechanism of model urethanes, J. Polym. Sci. Polym. Chem. Ed. 16 (1978) 213–228. https://doi.org/https://doi.org/10.1002/pol.1978.170160121.

[33] C. Petit, J. Bachmann, L. Michalek, Y. Catel, E. Blasco, J.P. Blinco, A.-N. Unterreiner, C. Barner-Kowollik, UV-induced photolysis of polyurethanes, Chem. Commun. 57 (2021) 2911–2914. https://doi.org/10.1039/D1CC00124H.

[34] M.M. Rahman, H.-D. Kim, W.-K. Lee, Properties of Waterborne Polyurethane Adhesives: Effect of Chain Extender and Polyol Content, J. Adhes. Sci. Technol. 23 (2009) 177–193. https://doi.org/10.1163/156856108X344667.

[35] F. Posada, J.-L. Gardette, Photo-oxidation of cured fluorinated polymers IV. Photo-oxidation of the fluorinated copolymer network with urethane linkage, Polym. Degrad. Stab. 70 (2000) 17–29. https://doi.org/https://doi.org/10.1016/S0141-3910(00)00064-1.

[36] X.F. Yang, C. Vang, D.E. Tallman, G.P. Bierwagen, S.G. Croll, S. Rohlik, Weathering degradation of a polyurethane coating, Polym. Degrad. Stab. 74 (2001) 341–351.

https://doi.org/https://doi.org/10.1016/S0141-3910(01)00166-5.

[37] C. Merlatti, F.X. Perrin, E. Aragon, A. Margaillan, Natural and artificial weathering characteristics of stabilized acrylic–urethane paints, Polym. Degrad. Stab. 93 (2008) 896–903. https://doi.org/https://doi.org/10.1016/j.polymdegradstab.2008.02.008.

[38] T. Endo, M. Kanamaru, T. Takata, Synthesis of poly(N-acylurethane)s, a new class of polyurethanes, Macromolecules. 27 (1994) 3694–3697. https://doi.org/10.1021/ma00092a002.

[39] M. Lazzari, O. Chiantore, Thermal-ageing of paraloid acrylic protective polymers, Polymer (Guildf). 41 (2000) 6447–6455. https://doi.org/https://doi.org/10.1016/S0032-3861(99)00877-0.

[40] O. Chiantore, M. Lazzari, Photo-oxidative stability of paraloid acrylic protective polymers, Polymer (Guildf). 42 (2001) 17–27. https://doi.org/https://doi.org/10.1016/S0032-3861(00)00327-X.

[41] J. Hioe, D. Šakić, V. Vrček, H. Zipse, The stability of nitrogen-centered radicals, Org. Biomol. Chem. 13 (2015) 157–169. https://doi.org/10.1039/C4OB01656D.

[42] Y. Feng, L. Liu, J.-T. Wang, S.-W. Zhao, Q.-X. Guo, Homolytic C−H and N−H Bond Dissociation Energies of Strained Organic Compounds, J. Org. Chem. 69 (2004) 3129–3138. https://doi.org/10.1021/jo035306d.

[43] M. Umar, M.I. Ofem, A.S. Anwar, A.G. Salisu, Thermo gravimetric analysis (TGA) of PA6/G and PA6/GNP composites using two processing streams, J. King Saud Univ. - Eng. Sci. (2020).

https://doi.org/https://doi.org/10.1016/j.jksues.2020.09.003.

[44] L. Feng, G. Li, X. Bian, Z. Chen, Y. Liu, Y. Cui, X. Chen, Rapid determination of residual monomer in polylactide using thermogravimetric analysis, Polym. Test. 31 (2012) 660–662. https://doi.org/https://doi.org/10.1016/j.polymertesting.2012.03.010.

[45] E.A. DiMarzio, On the Second-Order Transition of a Rubber, J. Res. Natl. Bur. Stand. Sect. A, Phys. Chem. 68A (1964) 611–617. https://doi.org/10.6028/jres.068A.059.

[46] D.W. Van Krevelen, K. Te Nijenhuis, Chapter 7 - Cohesive Properties and Solubility, in: D.W. Van Krevelen, K.B.T.-P. of P. (Fourth E. Te Nijenhuis (Eds.), Elsevier, Amsterdam, 2009: pp. 189–227. https://doi.org/https://doi.org/10.1016/B978-0-08-054819-7.00007-8.

[47] J. Delozanne, N. Desgardin, N. Cuvillier, E. Richaud, Thermal oxidation of aromatic epoxy-diamine networks, Polym. Degrad. Stab. 166 (2019) 174–187. https://doi.org/https://doi.org/10.1016/j.polymdegradstab.2019.05.030.

[48] NIST, NIST Chemistry WebBook, SRD 69, Diacetamide, (1988). https://webbook.nist.gov/cgi/cbook.cgi?ID=C625774&Mask=80#IR-Spec (accessed October 25, 2021).

[49] NIST, NIST Chemistry WebBook, SRD 69, Carbamic acid, phenol-, propyl ester, (2018). https://webbook.nist.gov/cgi/cbook.cgi?ID=C5532901&Units=SI&Mask=80#IR-Spec (accessed October 25, 2021).

[50] P. Cerruti, M. Lavorgna, C. Carfagna, L. Nicolais, Comparison of photo-oxidative degradation of polyamide 6,6 films stabilized with HALS and CuCl2+KI mixtures, Polymer (Guildf). 46 (2005) 4571–4583. https://doi.org/https://doi.org/10.1016/j.polymer.2005.03.065.

[51] B. Akih-Kumgeh, J.M. Bergthorson, Structure-reactivity trends of C1–C4 alkanoic acid methyl esters, Combust. Flame. 158 (2011) 1037–1048. https://doi.org/https://doi.org/10.1016/j.combustflame.2010.10.021.

[52] V. Saheb, S.M.A. Hosseini, Theoretical studies on the kinetics and mechanism of multi-channel gas-phase unimolecular reaction of ethyl acetate, Comput. Theor. Chem. 1009 (2013) 43–49. https://doi.org/https://doi.org/10.1016/j.comptc.2012.12.030.

[53] W.C. Danen, F.A. Neugebauer, Aminyl Free Radicals, Angew. Chemie Int. Ed. English. 14 (1975) 783–789. https://doi.org/https://doi.org/10.1002/anie.197507831.

[54] A. Tcharkhtchi, L. Audouin, J.M. Tremillon, J. Verdu, Oxyluminescence of polyamide 12, Polym. Degrad. Stab. 44 (1994) 335–341. https://doi.org/https://doi.org/10.1016/0141-3910(94)90092-2.

[55] V. Bellenger, J. Verdu, E. Morel, Structure-properties relationships for densely cross-linked epoxide-amine systems based on epoxide or amine mixtures, J. Mater. Sci. 24 (1989) 63–68. https://doi.org/10.1007/BF00660933.

[56] S. Terekhina, M. Mille, B. Fayolle, X. Colin, Oxidation induced changes in viscoelastic

properties of a thermostable epoxy matrix, Polym. Sci. Ser. A. 55 (2013) 614–624. https://doi.org/10.1134/S0965545X13090058.

[57] E. Richaud, X. Colin, C. Monchy-Leroy, L. Audouin, J. Verdu, Polyethylene stabilization against thermal oxidation by a trimethylquinoleine oligomer, Polym. Degrad. Stab. 94 (2009) 410–420. https://doi.org/https://doi.org/10.1016/j.polymdegradstab.2008.11.018.

[58] K. OGAWA, Y. NOMURA, Chemistry of Aminyl and Ammoniumyl Radicals, J. Synth. Org. Chem. Japan. 36 (1978) 342–351. https://doi.org/10.5059/yukigoseikyokaishi.36.342.

[59] S. Korcek, J.H.B. Chenier, J.A. Howard, K.U. Ingold, Absolute Rate Constants for Hydrocarbon Autoxidation. XXI. Activation Energies for Propagation and the Correlation of Propagation Rate Constants with Carbon–Hydrogen Bond Strengths, Can. J. Chem. 50 (1972) 2285–2297. https://doi.org/10.1139/v72-365.

[60] E. Richaud, B. Fayolle, J. Verdu, J. Rychlý, Co-oxidation kinetic model for the thermal oxidation of polyethylene-unsaturated substrate systems, Polym. Degrad. Stab. 98 (2013) 1081–1088. https://doi.org/https://doi.org/10.1016/j.polymdegradstab.2013.01.008.

[61] B.F. Sagar, Autoxidation of N-alkyl-amides. Part II. N-alkyl-amide hydroperoxides and di-N-alkyl-amide peroxides, J. Chem. Soc. B Phys. Org. (1967) 428–439. https://doi.org/10.1039/J29670000428.

[62] D.W. Van Krevelen, K. Te Nijenhuis, Properties of Polymers: Chapter 18-Properties Determining

Mass Transfer In Polymeric Systems, fourth edi, Elsevier, Amsterdam, 2009.

[63] E. Ernault, E. Richaud, B. Fayolle, Thermal-oxidation of epoxy/amine followed by glass transition temperature changes, Polym. Degrad. Stab. 138 (2017) 82–90. https://doi.org/https://doi.org/10.1016/j.polymdegradstab.2017.02.013.

[64] M.E. Nichols, J.L. Gerlock, Rates of photooxidation induced crosslinking and chain scission in thermoset polymer coatings II. Effect of hindered amine light stabilizer and ultraviolet light absorber additives, Polym. Degrad. Stab. 69 (2000) 197–207. https://doi.org/https://doi.org/10.1016/S0141-3910(00)00061-6.

Figure Captions

Fig. 1. (a) Structural units of acrylic polyol and (b) chemical structure of crosslinker (HDI trimer).

Fig. 2. Time-dependent IR spectra for thermally aging AUN at (a), (b) 200 °C; (c), (d) 180 °C; and (e), (f) 160 °C under air.

Fig. 3. Mass-loss behaviors under thermal aging at 160 °C, 180 °C, and 200 °C for AUN and polyol under air and vacuum (closed symbols correspond to AUN, open symbols to polyol).

Fig. 4. Evolution of T_g under thermal aging: (a) comparison of T_g changes at 200 °C under air and vacuum conditions, as assessed by DSC; and (b) temperature dependence of T_g evolution, as assessed by DMA.

Fig. 5. Swelling degree of virgin/aged AUN at 200 °C under air.

Fig. 6. Representative stress–strain curves for virgin/aged AUN.

Fig. 7. Plot of toughness vs. the concentration of imide (lower) and T_g values (upper) before/after AUN aging under air/vacuum (solid line and solid dot line denote linear fit regression of toughness vs [Imide] and toughness vs glass transition temperature, respectively).

Fig. 8. Changes with respect to aging time in the concentration of (a) imide, (b) PH, and (c) NH between 180 °C and 200 °C. The simulation curves and experimental data are presented as solid lines and open symbols, respectively.

Fig. 9. Simulation of the changes in the concentration of $[2X - 3S]$ under air (at 160 °C, 180 °C, and 200 °C) and vacuum (at 200 °C) conditions.